

Supplementary Information

Simultaneous Electronic and Ionic Conduction in Ionic Liquid Imbibed Polyacetylene-Like Conjugated Polymer Films

Arvind Sreeram,^a Sitaraman Krishnan,^{*a} Stephan J. DeLuca,^b Azar Abidnejad,^{‡a} Michael C. Turk,^c Dipankar Roy,^c Elham Honarvarfard^d and Paul J. Goulet^d

^a Department of Chemical and Biomolecular Engineering, Clarkson University, Potsdam, New York, 13699, USA. E-mail: skrishna@clarkson.edu; Fax: +1-315-268-6654; Tel: +1-315-268-6661

^b Energy Materials Corporation, Norcross, Georgia, 30071, USA

^c Department of Physics, Clarkson University, Potsdam, New York, 13699, USA

^d Department of Chemistry and Biomolecular Science, Clarkson University, Potsdam, New York, 13699, USA

[‡] Currently at Solvay USA Inc., Vernon, Texas, 76384, USA

Film surface morphology. Scanning electron microscopy of the ionic liquid containing conjugated polymer film showed a relatively uniform surface (see Fig. S1). No droplets of IL were evident on the film surface.

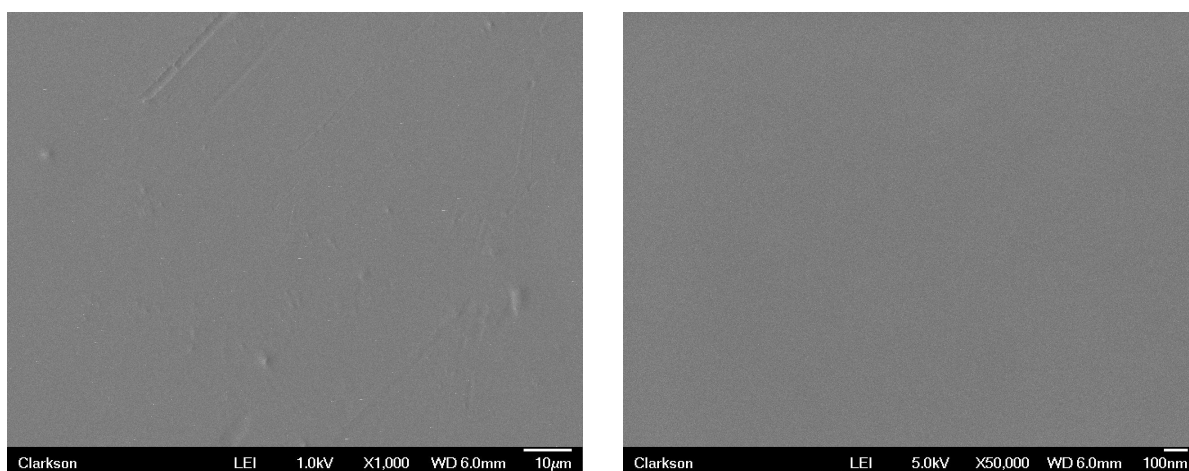
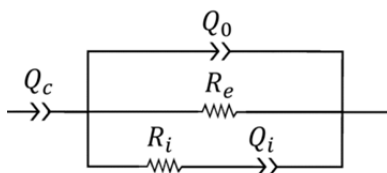


Fig. S1 Low magnification (1000 \times , left) and high magnification (50,000 \times , right) SEM images of film F2 after reaction at 200 °C. A photograph of the film is shown in Fig. 5 of the main article.

Detailed analysis of electrochemical impedance spectroscopy data. The electrical equivalent circuit (EEC) determined from the experimental impedance data is shown in Fig. 10 of the main article and is reproduced here.



The values of the parameters associated with the main elements of this circuit (Q_0 , R_e , R_i and Q_i) are summarized in Table S1. Y_0 and n_0 are parameters of the geometric constant phase element (CPE), Q_0 , and serve to define the impedance, $Z(Q_0)$, of the CPE as $Z(Q_0) = 1/[Y_0(j\omega)^{n_0}]$, where $j = \sqrt{-1}$. Likewise, Y_i and n_i are the CPE parameters of Q_i , and this CPE has the impedance, $Z(Q_i) = 1/[Y_i(j\omega)^{n_i}]$. Both the resistances, R_e and R_i , increase with decreasing temperatures, and the CPE parameters also show their expected temperature dependent behaviors.¹

Table S1 Temperature variation of the parameters of the EEC model determined by complex nonlinear least squares (CNLS) fitting of the EIS data acquired at 7 different temperatures.

T (°C)	115	100	85	70	55	40	25
$Y_0 \times 10^4$ (mS s ^{n_0})	5.62	17.6	25.8	5.73	1.09	0.293	0.156
n_0	0.5467	0.4935	0.4221	0.4794	0.5552	0.6059	0.5893
R_e (k Ω)	1.052	1.998	11.58	50.27	301.7	991.7	8224.0
R_i (k Ω)	0.319	0.979	6.33	26.06	109.9	741.3	5822.9 ^(a)
$Y_i \times 10^4$ (mS s ^{n_i})	2480	4800	107	72.2	38.5	5.78	n.d. ^(a)
n_i	0.4065	0.6705	0.6022	0.4575	0.3074	0.3093	n.d. ^(a)
f_{0e} (kHz) ^(b)	127.9	14.96	0.6537	0.2599	0.07517	0.05468	0.005209

^(a) not determined. At 25 °C, the net impedance of the R_i - Q_i branch was much larger than the net impedance of the Q_0 - R_e parallel combination, and hence could not be adequately resolved by CNLS fitting of the experimental data. However, the Q_0 - R_e unit was fully resolved at this temperature, and the corresponding parameter values are shown in the table. The value of R_i at 25 °C was determined by the method of extrapolation.

^(b) Characteristic frequency of the Q_0 - R_e subunit of the EEC. See the discussion that follows.

The impedance parameters shown in the last column of Table S1 are comparable, in their respective orders of magnitudes, to those previously reported for similar experimental systems involving mixed electronic and ionic conducting materials.^{2,3} The power-factor (n_0 or n_i in the present case) of the CPE varies between 0 and 1, with purely resistive and purely capacitive behaviors of the element emerging at these bounds, respectively.⁴ At a value of 0.5, this parameter represents a Warburg diffusion element.⁵ Based on the n_i values listed in Table S1, we identify the CPE, Q_i , to be a Warburg-like diffusion element, which along with the circuit element R_i , represents diffusion of ions. Because the current collector electrodes are ionically blocking, the ion transport should correspond to the case of restricted diffusion with reflective boundaries.⁶ Nevertheless, the observed CPE signature of Warburg-like semi-infinite diffusion implies that the diffusion frequency of the charge carriers is small compared with all the perturbation frequencies used for EIS.⁷ The observed deviations of n_i from the value of 0.5 (expected for

an ideal Warburg element) is attributed to inhomogeneous distribution of diffusion sites in the sample.^{6,8}

Unlike the case of ions, electron transport in our measurements is associated with non-blocking boundaries, and therefore, the parameters of the (“electron leaking”) geometric CPE, Q_0 , are affected by the diffusive movements of electrons. The expected Warburg-like nature of Q_0 is validated by the values of n_0 , observed in the neighborhood of 0.5, as expected for a Warburg element. It is likely that, this Q_0 is a parallel combination of the actual geometric CPE with a Warburg-like CPE resulting from electron diffusion. The latter is expected to dominate the resulting value of such a combination, because the intrinsic Y_0 for these systems tends to be rather small (typically in the range between 10^{-11} and 10^{-9} S s^n),^{2,3} which makes the innate impedance of the geometric CPE very large. The effect of electron diffusion on the value of Y_0 is also suggested by the observed increase in the value of this parameter with temperature, consistent with an expected increase in the diffusion coefficient with an increase in temperature.

As seen in Fig. 9 of the main article, the Nyquist spectra recorded at the moderate temperatures displayed two visually separable impedance arcs formed by the $Q_0(R_e)$ and the (Q_iR_i) subunits of the EEC. The specific circuit-blocks linked to these individual arcs can be identified from a careful examination of the characteristic frequencies (or time constants) of the arcs. For a simple parallel combination of a resistor and a CPE, the characteristic frequency would appear at the top (maximum $-Z''$) of the depressed semicircle generated by the combined elements.⁹ However, with the mutually overlapping arcs observed in the present work, it was difficult to clearly locate these characteristic frequencies by simple inspection.

Therefore, in order to identify the electronic and ionic components of the recorded Nyquist plot at each temperature setting, we evaluated the characteristic frequency of the $Q_0(R_e)$ block using the CNLS-fitted parameters. Subsequently, we traced the observed frequency spectrum to locate the position of the corresponding data point (labeled by its frequency coordinate) on the given plot. The $Q_0(R_e)$ subunit of the EEC was specifically chosen for this analysis, because the impedance parameters of this block were fully resolved in the CNLS fits at all temperatures of measurement (Table S1). In addition, this combination of elements would lead to a well-defined, and hence readily identifiable, semicircle with whose center is located at an angle of $[(1 - n_0)\pi/2]$ below the Z' axis. Once the Nyquist feature for this impedance contribution of electronic conduction was identified, the remaining Nyquist feature could be readily linked to ionic conduction.

The time constant (τ_{0e}) and the corresponding characteristic frequency (f_{0e}) of the $Q_0(R_e)$ combination were calculated using:⁹

$$\tau_{0e} = (Y_0 R_e)^{1/n_0} = (2\pi f_{0e})^{-1}$$

Fig. S2 shows the temperature dependent variation of f_{0e} , calculated using the above equation and the CNLS-fitted values of Y_0 and R_e from Table S1. The observed increase in f_{0e} with an increase in temperature is dominated by the thermal response of R_e (which decreases with temperature), and this is consistent with previously reported behaviors for such relaxation frequencies.¹⁰ For all the Nyquist spectra, acquired at the seven different temperatures, the impedance data points corresponding to the calculated values of f_{0e} were found to be located on the arcs at the high-frequency end (left side) of the spectrum.

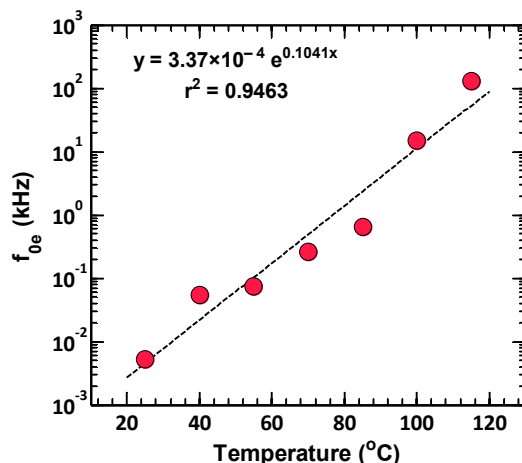


Fig. S2 Temperature dependence of the characteristic frequency, f_{0e} , of the Q_0 - R_e impedance unit in the EEC. The symbols represent data points obtained by CNLS fitting the experimental impedance data, and the solid trace is the best-fit curve for the f_{0e} vs. temperature data. The equation used and the overall quality of the fit (r^2 value) are indicated in the figure.

On the basis of this analysis, it was concluded that the arc associated with the higher frequency data (left side of the Nyquist spectrum) in Fig. 9 was linked to electronic conduction, while the arc corresponding to the lower frequency data (on the right side of the Nyquist plot) was associated with ionic conduction.

Shape of the Nyquist spectra acquired at 115 °C. The radius of the arc attributed to the electronic conduction is proportional to R_e .⁹ From the values of R_e given in Table S1, it is evident that the radius of this arc would decrease with an increase in temperature. Simultaneously, because of an increase in f_{0e} with temperature (cf. Fig. S2), the top of the arc would shift toward the left of the Nyquist spectrum, carrying with it the entire arc. At 115 °C, the top of the electronic arc was located at impedance values corresponding to 128 kHz, and therefore, at the very left end of the $+Z'$ axis. (Note that the last experimental data point observed at the left-most end of the $+Z'$ axis in each panel of Fig. 9 was from a measurement using a perturbation frequency of 300 kHz). As a result, only a small portion of the $Q_0(R_e)$ arc was revealed in our measurements (see the high-frequency corner of the Nyquist spectrum in Fig. 9D), while the remaining plot area was covered by the arc resulting from ionic conduction. Note also that the overall dimension of the ionic arc was significantly smaller for the spectrum acquired at 115 °C, compared with the ionic arcs observed in the lower temperature spectra. However, on the optimized impedance scale used in Fig. 9D, the Nyquist feature of the ionic rail appears to dominate the observed spectrum. In conclusion, the impedance spectrum collected at 115 °C was predominantly the signature of the ionic rail, whereas the spectrum acquired at 25 °C was, for most part, a manifestation of the electronic rail. The spectra acquired at intermediate temperatures displayed impedance features from both, the electronic and the ionic transport pathways.

References

1. J. R. Macdonald, *Solid State Ionics*, 1984, **13**, 147–149.
2. M. Wasiucionek, J. Garbarczyk, B. Wnętrzewski, P. Machowski and W. Jakubowski, *Solid State Ionics*, 1996, **92**, 155–160.
3. E. S. Matveeva, R. D. Calleja and V. Parkhutik, *J. Non-Cryst. Solids*, 1998, **235**, 772–780.
4. J. Jorcin, M. E. Orazem, N. Pébère and B. Tribollet, *Electrochim. Acta*, 2006, **51**, 1473–1479.
5. E. Cuervo-Reyes, C. P. Scheller, M. Held and U. Sennhauser, *J. Electrochem. Soc.*, 2015, **162**, A1585–A1591.
6. J. Bisquert, *J. Phys. Chem. B*, 2002, **106**, 325–333.
7. J. Garland, D. Crain and D. Roy, *Electrochim. Acta*, 2014, **148**, 62–72.

8. J. Bisquert and A. Compte, *J. Electroanal. Chem.*, 2001, **499**, 112–120.
9. G. J. Brug, A. L. G. Van Den Eeden, M. Sluyters-Rehbach and J. H. Sluyters, *J. Electroanal. Chem.*, 1984, **176**, 275–295.
10. J. R. MacDonald, *Solid State Ionics*, 1985, **15**, 159–161.